



Cardiac myxoma: a contemporary multimodality imaging review

Geoffrey C. Colin^{1,2} · Bernhard L. Gerber² · Mihaela Amzulescu² · Jan Bogaert¹

Received: 20 March 2018 / Accepted: 12 June 2018
© Springer Nature B.V. 2018

Abstract

Cardiac myxoma (CM) is by far the most common primary benign cardiac tumor, typically arising in the left atrium with an attachment point in the fossa ovalis region. Although the etiology of CM remains unclear, we know that this endocardial-based mass originates from undifferentiated mesenchymal cells. Continuous technical improvements in the field of echocardiography since the 1960s has profoundly changed the diagnostic approach by allowing a good tumor detection as well as the preoperative planning by providing crucial information concerning the attachment point location. However, echocardiography has its limitations among which lack of tissue characterization and restricted field of view can arise diagnosis difficulties in atypical presentations. With the widespread and routine use of echocardiography and chest computed tomography (CT), incidental detection of CM is not infrequent. As a consequence, it has become mandatory for cardiologists and radiologists evolving in a multimodality imaging world to be familiar with the wide range of presentations of this tumor. The authors present here a review of the common and less common aspects of CM using the main imaging modalities available: echocardiography, cardiovascular magnetic resonance imaging, CT, positron emission tomography and coronary angiography.

Keywords Cardiac magnetic resonance imaging · Echocardiography · Computed tomography · Cardiac mass · Oncology · Review

Abbreviations

CM	Cardiac myxoma
CMR	Cardiovascular magnetic resonance
CT	Computed tomography
IAS	Interatrial septum
LA	Left atrium
LGE	Late gadolinium enhancement
PET	Positron emission tomography
TTE	Transthoracic echocardiography
TEE	Transoesophageal echocardiography

T1w	T1-weighted
T2w	T2-weighted

Introduction

Cardiac myxoma (CM)—the most common primary benign cardiac tumor—accounts for 50–80% of clinical cases [1, 2] and approximately 70% of operated cases [3]. The diagnosis is often challenging owing to its heterogeneous clinical, radiological and histological features. Despite its rarity, CM should be considered in the differential diagnosis of dyspnoea, embolic events (mainly stroke), syncope, palpitations. Also, in patients with constitutional symptoms, including fever of unknown origin or weight loss, CM may be the underlying cause. Rarely, it may mimic endocarditis or cancer [4]. Although reported, diagnosis of CM made at autopsy has become nowadays an exception [5]. Historically, the emergence of angiography in 1952 allowed preoperative diagnosis [6], but the real break-through to noninvasively detect CM coincided with the advent of echocardiography in the 1960s [7], substantially improving pre-operative planning, surgical tumor resection with overall excellent long term survival rates [8]. Nowadays, the goal of

✉ Geoffrey C. Colin
gc.colin.md@gmail.com

Bernhard L. Gerber
bernhard.gerber@uclouvain.be

Mihaela Amzulescu
mihaela.amzulescu@uclouvain.be

Jan Bogaert
jan.bogaert@uzleuven.be

¹ Division of Radiology, Department of Imaging and Pathology, Medical Imaging Research Center, University Hospitals Leuven, Herestraat 49, 3000 Leuven, Belgium

² Division of Cardiology, Cliniques Universitaires Saint-Luc, Brussels, Belgium

imaging—apart from the detection of an abnormal intracardiac structure—is to tissue characterize the ‘mass’ providing more or less accurate information with regard to histology, and to exclude other potential diagnosis. In addition, imaging is needed to provide detailed information with regard to tumor insertion and relation of the heart to the chest as minimally invasive such as robotic surgery is increasingly used to treat cardiac patients.

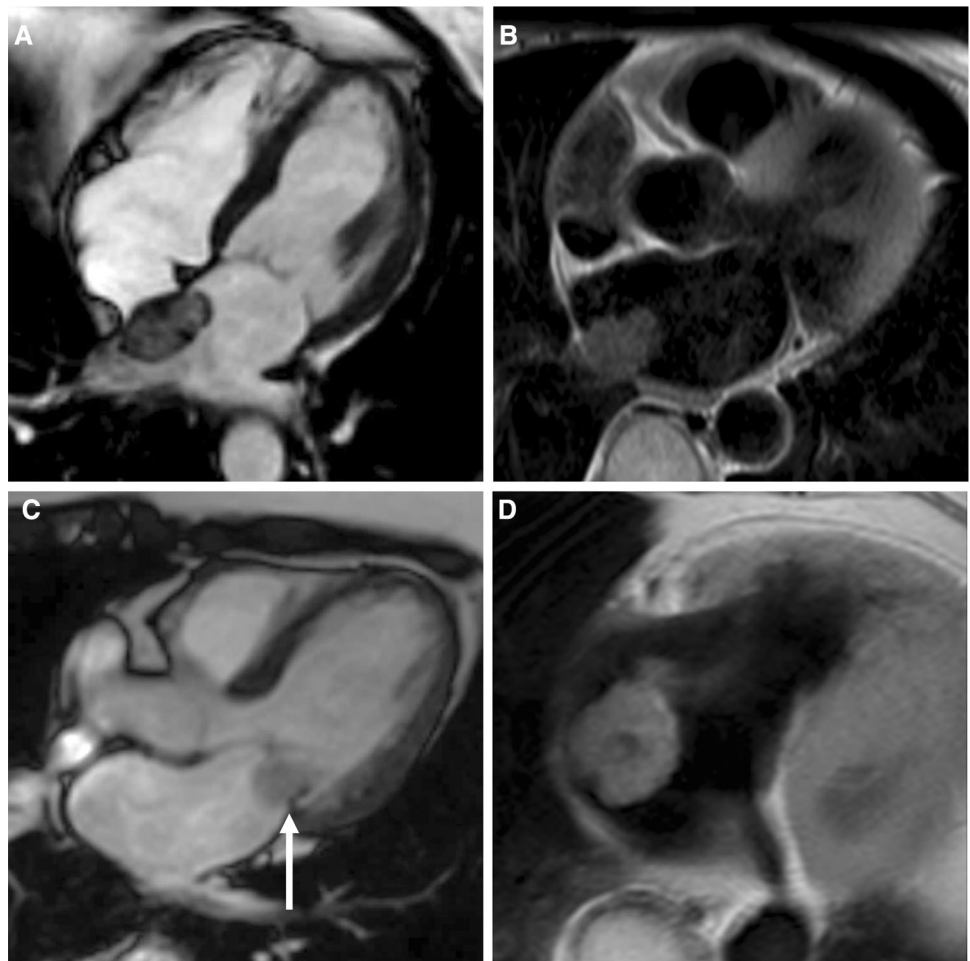
General features and relation with clinical, imaging and pathological findings

Main imaging characteristics of CM are summarized in Table 1. The vast majority of CM (80% of cases) are located in the left atrium [2] originating at the interatrial septum (IAS) (80% of cases) (Fig. 1a). Other locations include the posterior and lateral left atrial (LA) wall

Table 1 Characteristics of cardiac myxoma

80%	Interatrial septum attachment
80%	Left atrium location
50–80%	Of all primary cardiac benign tumors
Mobility	Landmark characteristic but inconstant in sessile tumors
30%	Obstructive through tricuspid or mitral valve
10–20%	Calcifications
Heterogeneous behavior and growth rate	
Echocardiography, CMR: heterogeneous aspect depending on hemorrhage, calcification and surface thrombus content	
CT, CMR: variable heterogeneous enhancement depending on tumor vascularization	
¹⁸ F-FDG PET: no or low ¹⁸ F-FDG uptake	

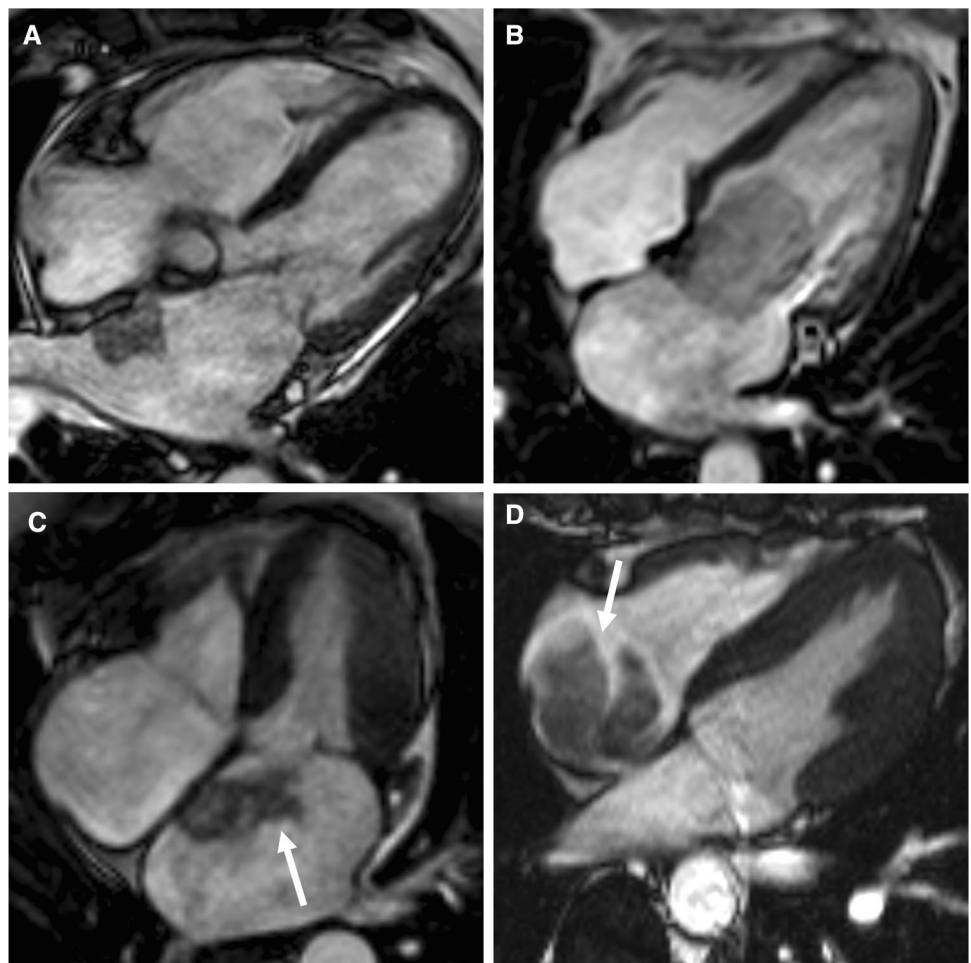
Fig. 1 The typical localization of CM is an attachment point on the interatrial septum (a). Atypical localizations include the pulmonary vein ostia (b), the mitral valve (c) and the right atrial posterolateral wall (d)



(including the pulmonary vein ostium), the left appendage, the mitral and tricuspid valve, the posterior right atrial (RA) wall and, exceptionally, the right, left ventricle and pulmonary artery [2, 9] (Fig. 1b–d). The endocardial attachment point is either broad, sessile or narrow, pedunculated. The latter are typically mobile—the degree of mobility depends on the length of the stalk—and they may prolapse across the atrioventricular valve during the diastole hereby restricting ventricular filling (Fig. 2a, b). The term “narrow stalk”, however, is prone to discussion and likely responsible for the great differences reported in the literature on the percentage of pedunculated tumors (range 30–85%) [2, 10]. Although CM has a mean size of 3–4 cm according to recent publications, tumor size can be highly variable [11, 12]. Tumor size determines its mobility as well as its potential for obstructing the atrioventricular valve [4]. Tumor contours are either smooth or lobulated (most common), or irregular, with villous expansion or even fragmented presentation [3, 7, 13, 14] (Fig. 2c, d). The latter is associated with a higher embolic event rate [2, 10, 13, 15]. It is important to emphasize that

embolic events are not size-related [10] and frequently occur in small tumors as well [16]. This concept is supported by the fact that the rate of embolic presentation (10–20%) is nearly unchanged since the first publications on CM despite the ability to detect much smaller lesions with modern invasive modalities. Myxomas are non-invasive and thus do not reach the epicardial part of the cardiac wall. As a consequence, pericardial involvement (e.g. effusion) is not part of the spectrum of CM. Histologically, myxomas have a myxoid matrix with embedded myxoma cells. Frequently, the tumour contains areas of (ancient) haemorrhage with pigmented macrophages and hemosiderin, as well as intratumoral calcifications (9–17%) [2, 3]. Finally, the tumor surface may be covered by a thrombus. As discussed more extensively in the following paragraphs, tumor histology determines imaging features (Fig. 3). Myxomas are considered a benign tumor with a variable vascularization and growth rate (Fig. 4). A mean growth rate of 4–5 mm/month has been reported [17]. However, some found nearly unchanged dimensions for several years [18, 19] while others reported

Fig. 2 The attachment point to the endocardium can be broad (sessile tumor, **a**) or with a stalk (pedunculated tumor, **b**). The latter presents mobility during the cardiac cycle with potential prolapses through the atrioventricular valve during the diastole. CM are generally well-defined lesions with round or lobulated shape (**a**, **b**). However, the lesion may be irregular with villous expansion (**c**, white arrow) or be fragmented (**d**, white arrow)



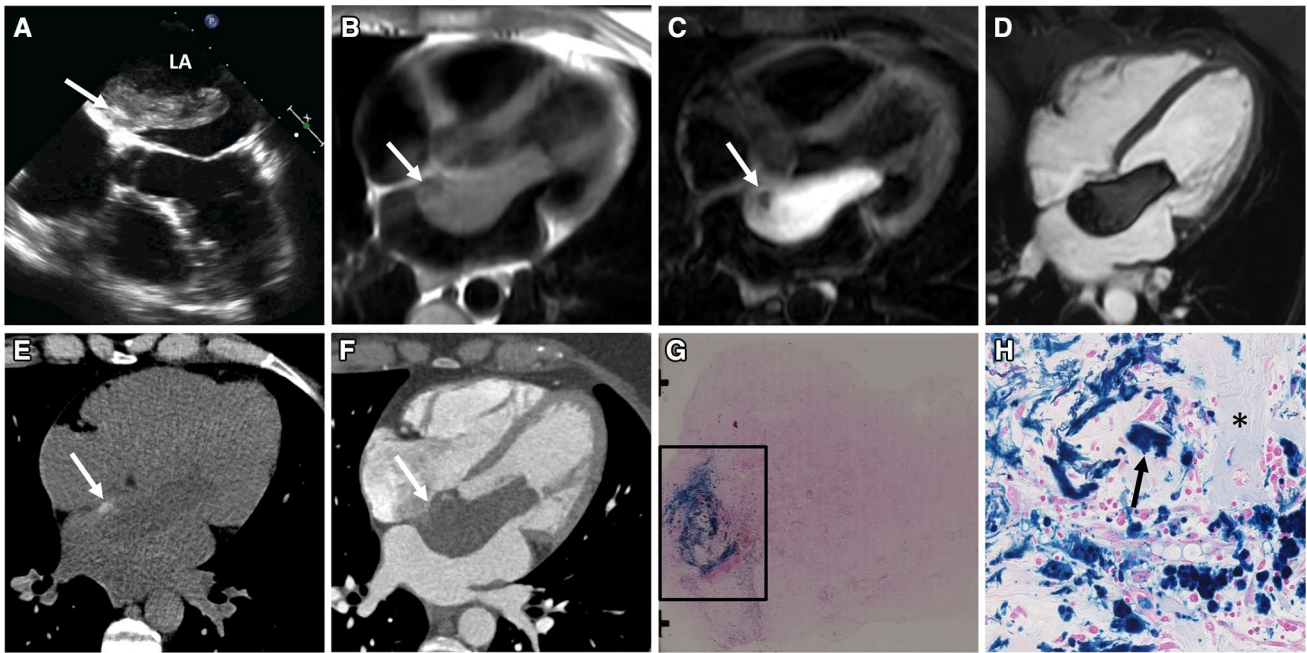
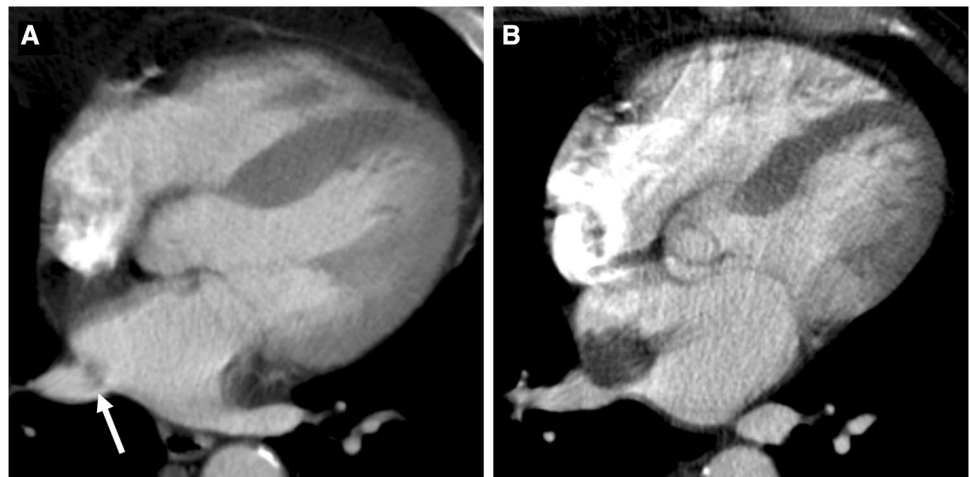


Fig. 3 Typical presentation of a CM in the left atrium (LA). TEE (a) demonstrated a hyperechoic area nearby the attachment point on the interatrial septum (arrow). At CMR, the mass was isointense at T1w (b) and hyperintense at T2w (c) imaging, with a nodular hypointensity nearby the attachment point on the interatrial septum (arrows). LGE images demonstrated no significant enhancement (d). Cardiac CT showed a homogenous mass (29 HU), with a punctiform calcification (arrow) (e) and no enhancement (f). At histology, Pearls stain-

ing showed the presence of hemosiderin in macrophages and calcifications nearby the attachment point (g, magnification $\times 0.36$, left part of the image), while the main part of the tumor was a homogenous myxomatous tissue (light pink). Magnification at $\times 40$ (h) better showed the presence of hemosiderin in macrophages (arrows) and calcifications in Gamma-Gandy bodies (*). These findings matched with the hypointense area in CMR images

Fig. 4 68-year-old patient with recent history of oral squamous cell carcinoma. At the follow-up CT, a small mass appeared in the left atrium near the right inferior pulmonary vein and was initially missed (a, arrow). One year later, the mass measured 35 mm with villous expansion (b). After CMR findings (not shown), a surgical resection revealed a myxoma



high growth rates mimicking malignant processes [20]. Rarely, CM may present atypical at histology showing the presence of mitoses or pleomorphic cells that could lead to misdiagnosing CM as a malignancy such as sarcoma (“malignant myxoma”) [2, 21].

Imaging modalities

First described at autopsy in 1854, pre-mortem diagnosis of CM was only achieved in 1952 with the use of angiography [6]. First echocardiographic detection of myxoma was reported in literature in 1959 [22] and made a profound impact on detection and management of myxoma. More recent imaging modalities include computed tomography (CT) first reported in 1978 [23], cardiovascular magnetic resonance imaging (CMR) in 1984 [24] and positron emission tomography (PET) in 1999 [25].

Angiography

Before the introduction of cardiac ultrasound, angiocardiology with left heart catheterization was the only imaging modality allowing preoperative diagnosis in 78% of cases [26]. In 1969, tumor vascularity in LA myxoma was demonstrated by selective coronary arteriography [27]. In 31–56% of patients, cardiac catheterization shows a

tumor blush [2, 28–30]. Given its posterior localization, CM is commonly supplied by either the right coronary or the left circumflex artery (Fig. 5). Tumor neovascularization is not specific of CM and can be encountered in other primary cardiac tumors such as angiosarcoma or paraganglioma.

Echocardiography

Until the 1970s, M-mode transthoracic echocardiography (TTE) was the only available method to depict CM. Nowadays two-dimensional TTE is the first and most frequently used imaging technique to detect this tumor. TTE accurately defines the location, size, shape, attachment, and mobility of CM as well as hemodynamic consequences. The appearance may be homogenous or heterogeneous [16] with presence of calcifications in less than 10% of cases—not infrequently without a retro-acoustic shadow (Figs. 3, 6, 9). Pure cystic forms have been seldomly reported as well [31, 32] (Fig. 7). Rarely, vascularization can be demonstrated at color-Doppler imaging [33].

Suboptimal image quality at TTE, due to poor echogenicity, may hamper CM detection in up to 5% of patients [26]. Moreover, the exact location of the attachment point may be impeded, especially in RA myxoma. Transoesophageal echocardiography (TEE) with high frequency transducers (7 MHz) improves spatial resolution. The proximity of the transducer to the atria improves the ability to characterize

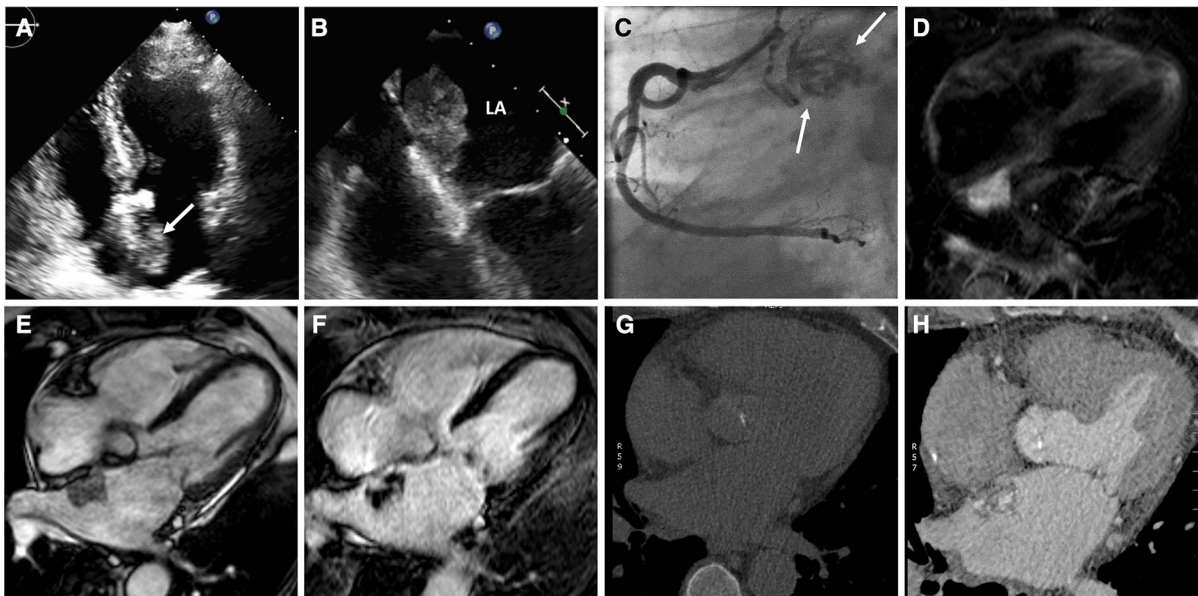


Fig. 5 Highly vascularized myxoma in an asymptomatic 84-year-old woman. TTE (a) revealed a sessile mass (arrow) in the left atrium (LA) with an interatrial septum attachment and was better visualized at TEE (b). Coronary angiography showed abnormal vessels arising from the right coronary artery (c, arrows). CMR showed a mass

hyperintense at T2w imaging (d), hyperintense with punctiform area of hypointensity at cine imaging (“blackberry” appearance) (e) and a heterogeneous enhancement at LGE imaging (f). Myxoma was not visible at cardiac CT before contrast medium injection (g) and after showed a strong enhancement (h)

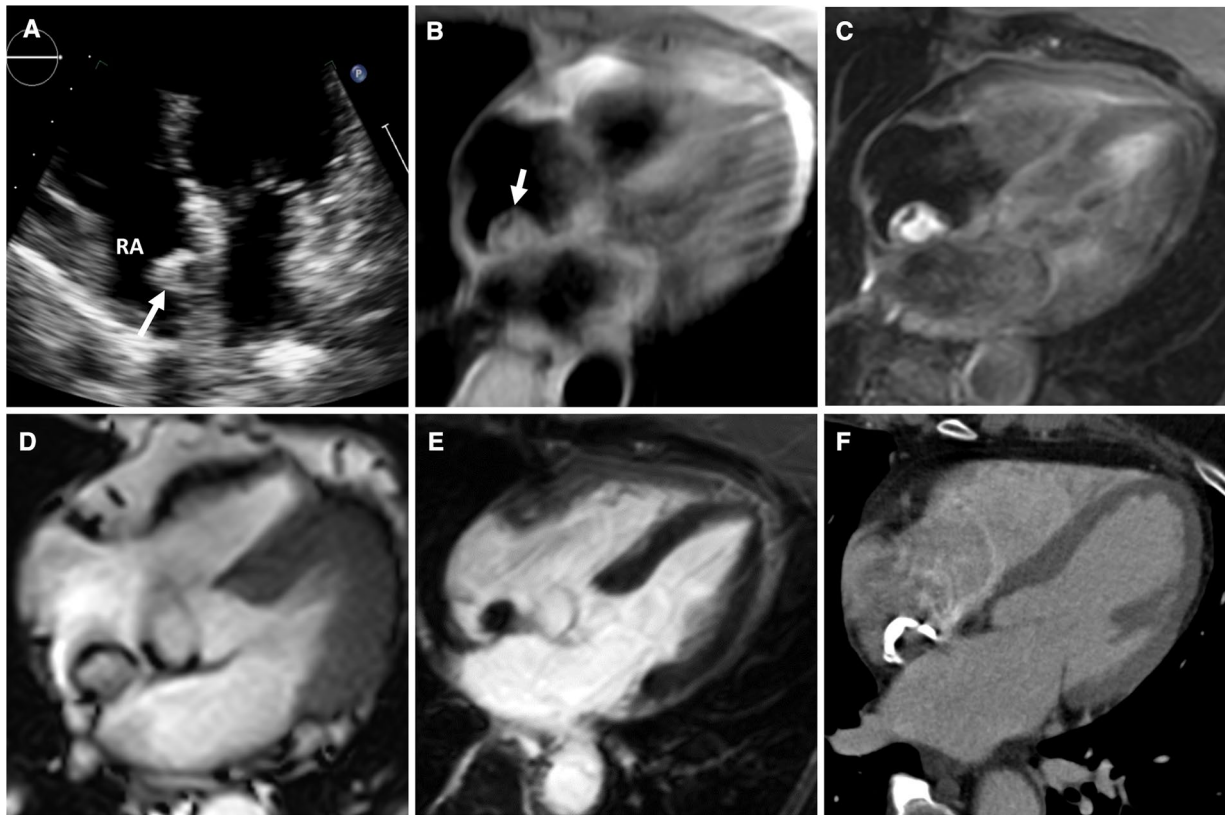


Fig. 6 Calcified myxoma. A 16×10 mm hyperechoic right atrial (RA) mass was discovered in a 61-year-old asymptomatic woman during routine TTE (a). The mass was isointense at T1w (b), hyperintense at T2w (c) and cine imaging (d) with a peripheral hypointense

rim. There was no contrast agent uptake at LGE imaging (e). The hypointense rim corresponded to peripheral calcifications who were only well demonstrated by cardiac CT (f)

the tumor appearance, dimensions and location [34] (Fig. 5a, b). Hence, TEE is superior to TTE for myxoma detection (100% vs 95%) and attachment point identification (95.2 vs 64.5%) [26], especially for RA myxomas [35, 36]. More recent improvements in echocardiography include perfusion imaging and 3D imaging. Quantitative perfusion imaging may be helpful to demonstrate differences of perfusion patterns between malignancies (hyperenhancing pattern), benign stromal tumors (hypoenhancing pattern) and thrombus (non-enhancing pattern) [37–39]. However, the diagnostic yield of perfusion imaging is still limited to differentiate within the group of poorly vascularized masses (e.g., myxoma and thrombus) and the group of highly vascularized masses (e.g. sarcoma and hemangioma). Finally, 3D echocardiography provides valuable information about shape, site of attachment, and surface characteristics of intracavitary masses compared to 2D echocardiography [40].

Cardiovascular magnetic resonance imaging

As CMR is comprehensive, it may provide valuable information with regard to the diagnosis and differential diagnosis of cardiac masses, and is therefore increasingly used in the diagnostic work-up of CM. At pre-contrast T1-weighted (T1w) and T2-weighted (T2w) CMR, myxoma exhibits three different patterns. The most frequent presentation is a mass isointense at T1-weighted (T1w) and hyperintense at T2-weighted (T2w) imaging with foci of hypointensity at one or two of these sequences [14]. At steady-state free precession (SSFP) cine imaging, the association of punctiform area of high and low signal intensity might sometimes give a “blackberry” appearance (Figs. 1a, 2a). A second pattern includes marked low signal intensity at T1w, T2w and cine imaging, a pattern that potentially can mimic a thrombus (Figs. 8, 9). This presentation seems to be more frequent

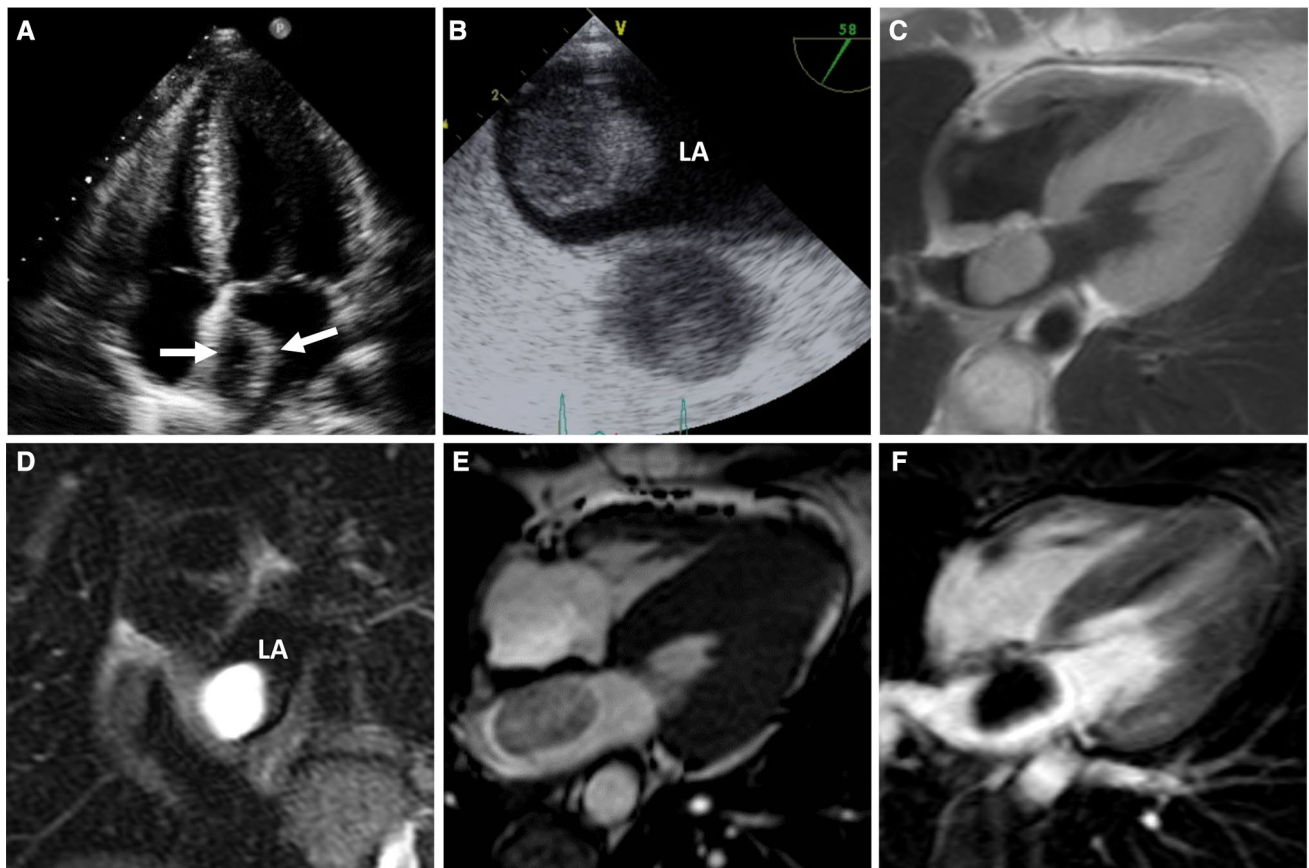


Fig. 7 Pseudocystic myxoma. TTE (a) and TEE (b) showed a sessile mass in the left atrium (LA) with interatrial septum attachment and cyst appearance. CMR presentation was also unusual with a homogenous isointense signal intensity at T1w imaging (c) and very high

signal intensity at T2 imaging (d). Cine imaging (e) showed a hyperintense mass with a mild punctiform heterogeneity (“blackberry” appearance). There was no contrast agent uptake at LGE imaging (f)

in RA myxomas and could histologically be explained by a higher calcification content [2]. A third possible presentation is a homogenous mass with markedly hyperintense appearance at T2w imaging (sometimes giving the tumor ‘pseudocystic’ appearance) (Fig. 7). The pre-contrast CMR presentation can be explained by its’ histology. Hyperintensity at T2w and cine imaging is related to its myxoid matrix with high water and polysaccharide content, while foci of hypointensity (in variable amount) are related to area of haemorrhage, hemosiderin (degradation of haemoglobin), calcifications or surface thrombus. With the use of older gradient-recalled echo cine images, CM were frequently hypointense at cine imaging due to the susceptibility effects of these components [41–43]. With SSFP imaging, tissue contrast mostly depends on the T2/T1 ratio and therefore myxoma are typically hyperintense relative to the myocardium at cine imaging [44, 45]. The use of gradient-echo T2*

images may better show susceptibility artefacts due to hemosiderin content (Fig. 10a, b) [46]. However, this sequence suffers from considerable artefacts and image quality is often poor, limiting its use in clinical practice. Cine imaging is the most appropriate sequence to determine the attachment point and the tumor mobility. Tumor prolapse through the mitral valve has been reported in 30% of cases. Optionally phase contrast imaging in the plane of mitral valve may be useful to assess inflow obstruction and to calculate the reduction of the mitral valve orifice (Fig. 10c, d). At first-pass perfusion imaging, myxoma show enhancement in 16–66% of cases [14, 47], which however, is often weaker than the normal myocardium (hypoperfused enhancement pattern) [48, 49] (Fig. 11). Moreover, interpretation of perfusion patterns (such as perfusion slope analysis) may be severely impeded in mobile myxomas. In about half of patients, heterogeneous (patchy or peripheral) enhancement is shown at

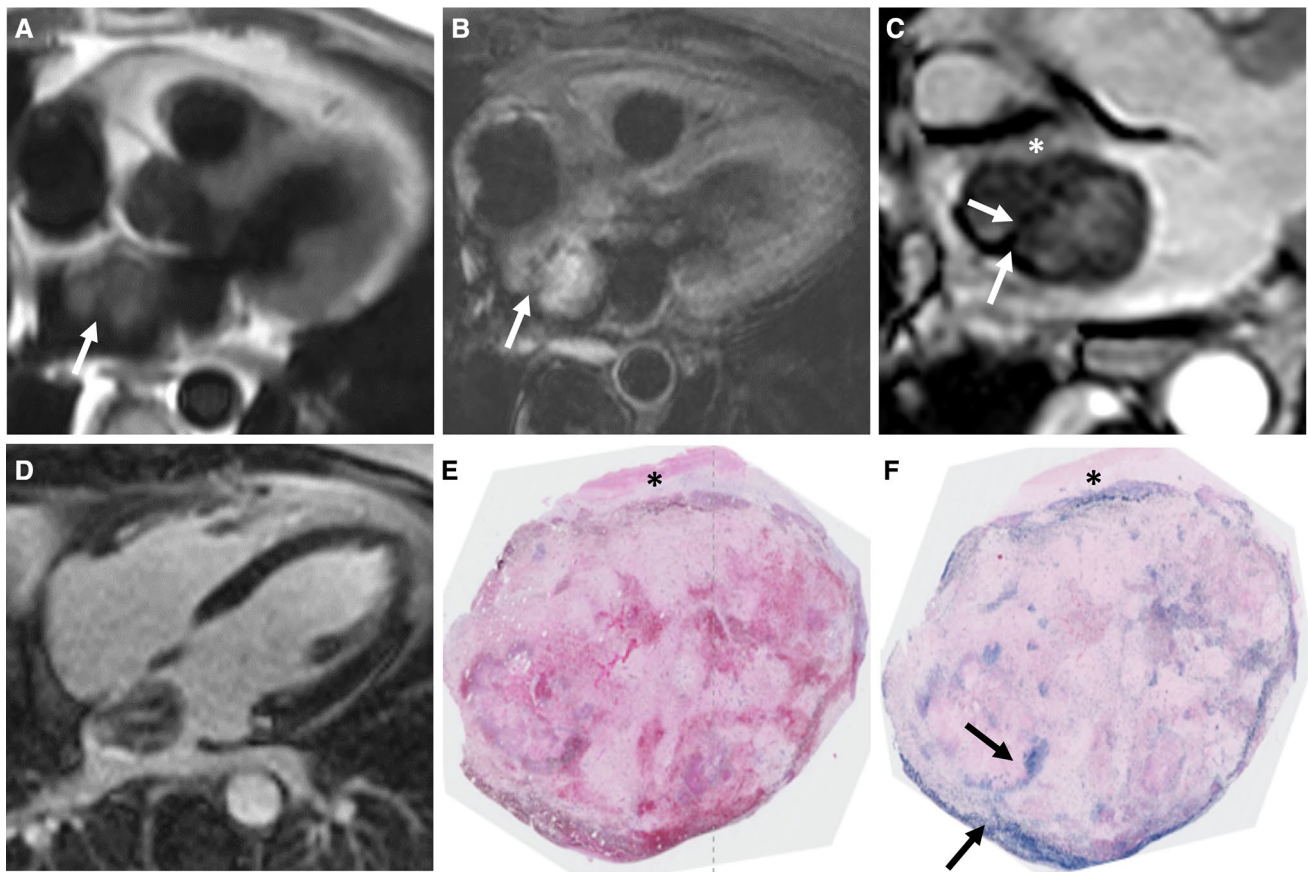


Fig. 8 Hemorrhagic myxoma. CMR showed a mass with heterogeneous signal intensity at T1w (a), T2w (b) and cine (c) imaging with area of hypointensity (arrows). The interatrial septum attachment point was correctly identified on cine imaging (*). LGE imaging showed heterogeneous enhancement (d). Histological examina-

tion revealed large hemorrhage area (e, Hematoxylin-Eosin staining, magnification $\times 0.46$) and high hemosiderin content (f, Pearl staining, magnification $\times 0.46$). In that case, the deposit of hemosiderin in Pearl staining perfectly matched the hypointense rim at cine imaging

late gadolinium enhancement (LGE) imaging. In myxomas showing weak or no enhancement at LGE differentiation with thrombus may be challenging [14]. Use of longer inversion times at LGE (e.g. 550–600 ms) of post-contrast T1w imaging may be recommend to show contrast enhancement in these cases (Fig. 10d, e). In our experience, we could not find a relation between pre-contrast imaging features (T1w, T2w and cine imaging) and LGE enhancement patterns. Recent advances in CMR include parametric techniques (T1 and T2 mapping) providing quantitative data with regard to tissue relaxation times. Although designed and normally used for myocardial tissue characterization, these sequences can be applied to characterize cardiac tumors (Fig. 12). Two recent studies showed T1 times varying between 1285 and 1356 ms and T2 times varying between 76 and 270 ms for CM at 1.5 T [50, 51].

Computed tomography (CT)

At unenhanced CT, myxoma frequently appears homogeneous and isodense or slightly hypodense relative to the blood (average attenuation : 22 Hounsfield Unit (HU)) [52]. After iodine contrast medium injection, tumor enhancement is often weak or absent, with a mean attenuation reported about 43 HU [11]. However, CM may show high enhancement in some cases (Fig. 3). In most of cases, attenuation of myxoma on both pre-contrast and post-contrast injection images is not sufficient to differentiate myxomas from thrombi [11]. Therefore, the interest of CT in CM diagnosis is limited. However, CT is the preferred technique to detect calcifications (10–30% of cases) [43, 52]. Furthermore, the development of dual-energy technique could improve differentiation between CM and thrombi. This technique

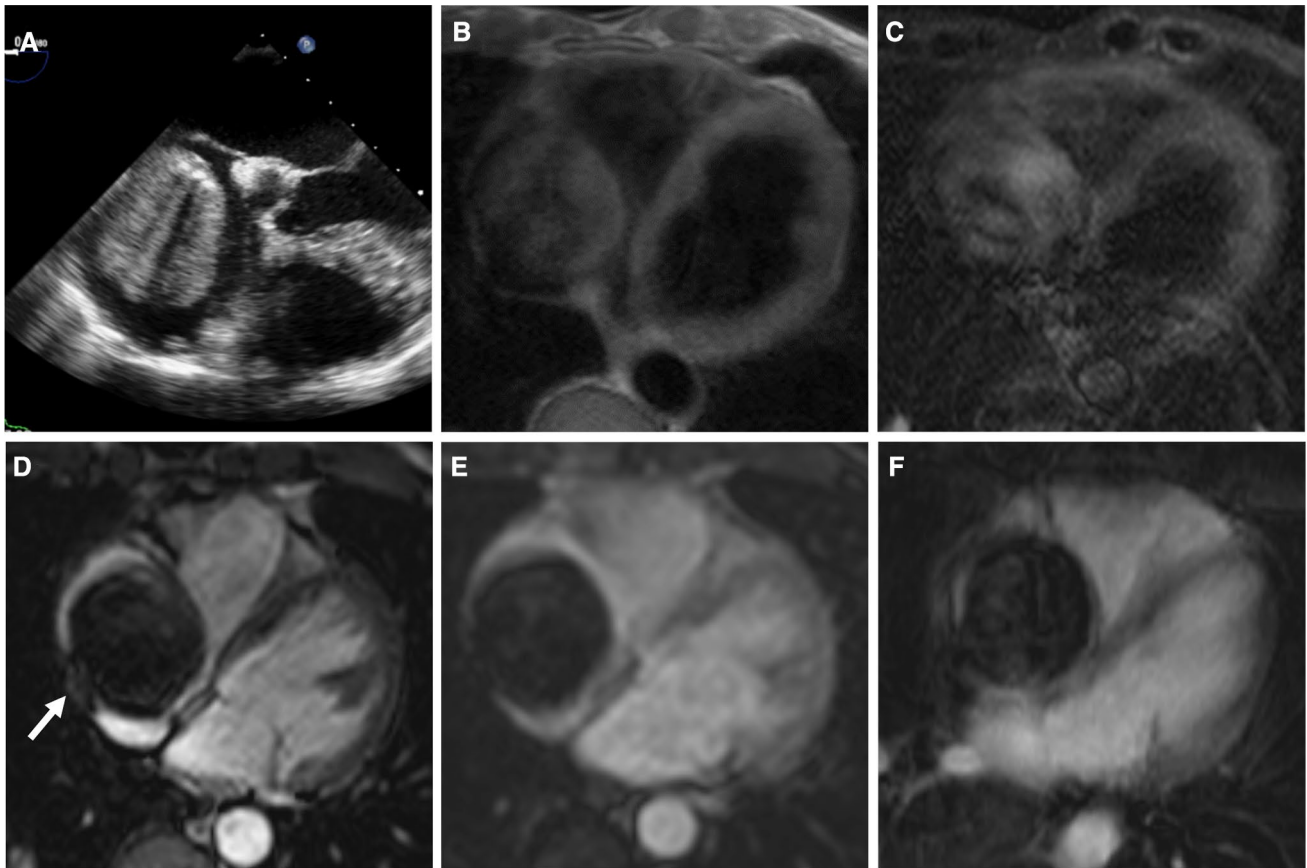


Fig. 9 Cardiac myxoma mimicking thrombus. TEE showed a right atrial (RA) mass with acoustic shadowing and the attachment point could not be precisely determined (a). At CMR, myxoma was hypointense at T1w (b), T2w (c) and cine (d) imaging and no noticeable

contrast agent uptake was discerned at both perfusion (e) and LGE (f) imaging. Cine imaging also correctly identified the attachment point on the posterior right atrial wall (arrow). Histology revealed myxoma with high hemosiderin and calcifications content

highlights the contrast-enhanced structures by measuring their iodine concentrations after iodine contrast medium injection. In their study, Hong et al. demonstrated a significant higher iodine concentration in myxomas than in thrombi [12].

¹⁸F-FDG PET

Experience of fluorodeoxyglucose positron emission tomography (¹⁸F-FDG PET) in cardiac tumors is rather limited. Most CM show no or low ¹⁸F-FDG uptake with standard uptake value (SUV) varying from 1.2 to 5.3 [53] (Fig. 13). The reason why some myxomas show ¹⁸F-FDG uptake while others do not remains unclear [54]. Beyond myxomas, in selected cases ¹⁸F-FDG PET may be of interest in the diagnostic work-up of cardiac masses [55, 56]. A few pitfalls—mainly concerning false positive findings—with ¹⁸F-FDG PET should be kept in mind. In particular, lipomatous hypertrophy of the interatrial septum frequently demonstrates mild ¹⁸F-FDG uptake due to brown

fat activation [57]. The association with CT/MRI findings remains essential to demonstrate the lipomatous nature of this pseudotumor. Cardiac paraganglioma may also show high ¹⁸F-FDG uptake [58]. Finally, inflammatory or infectious tumors may also be ¹⁸F-FDG avid lesions and mimic a malignant cardiac mass [59].

Differential diagnosis and impact of imaging on clinical management

Theoretically, the list of ‘cardiac masses’ mimicking myxomas is large. Based on tumor characteristics, cardiac imaging has the potential to choose the optimal patients’ treatment: surgical removal of the mass, anticoagulant therapy, oncologic therapy (chemotherapy, radiotherapy) or conservative management with or without follow-up [47]. Given the risk of embolic events, heart failure or even sudden death and the potential high growth rate [60] a confident diagnosis is crucial when CM is suspected, for immediate treatment.

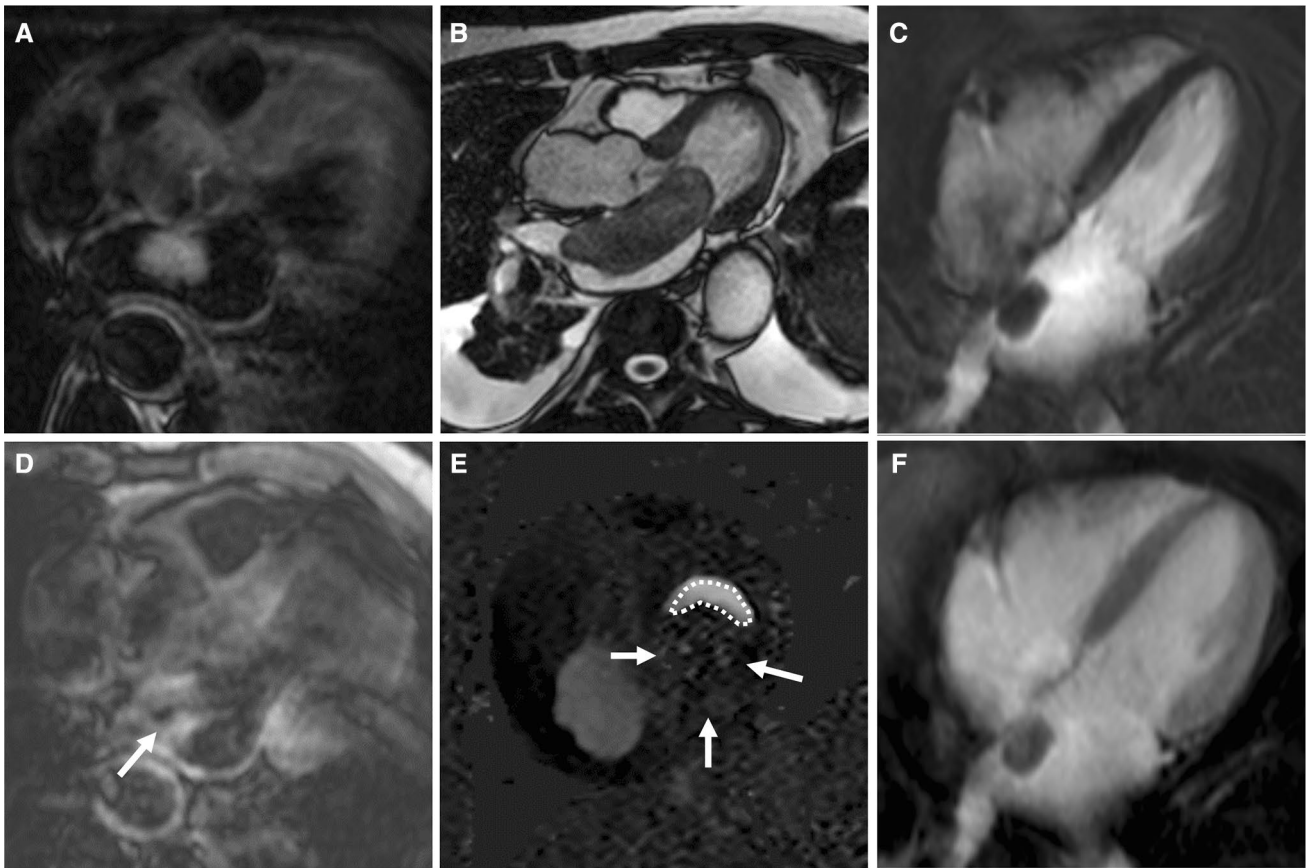


Fig. 10 Optional CMR sequences. (a, b) While fast-spin echo T2w imaging may be limited in demonstration area of hypointensity (a), the use of gradient-echo T2* imaging with longer echo-time (b) increases the susceptibility of the sequence and the demonstration of area of hemorrhage. (c, d) The atrioventricular valve obstruction can be seen at cine imaging (c) or can be assessed by the phase contrast

sequence (d) in the valve plane allowing calculation of the induced mitral valve stenosis (discontinued points) by the prolapse of the myxoma (arrows). (e, f) Myxoma may be hypointense on LGE imaging with usual inversion times (e, 240–330 ms), but become hyperintense with use of longer inversion time (f, 550 ms), allowing differentiation with thrombus

The main differential diagnosis of cardiac myxoma with IAS attachment is reported in Table 2.

Anatomic variant and pseudotumors do not infrequently cause false positive diagnosis at TTE and represent a significant portion of patients referred for CMR [61] (Figs. 14, 15), including lipomatous hypertrophy of the IAS, mitral valve annulus (caseous) calcification, prominent crista terminalis or IAS aneurysm. CMR, as well as CT, are reliable techniques to identify these pseudotumors (e.g. by showing anatomic location or fat or calcified content) and can provide a definitive diagnosis [62].

Thrombi are often the first alternative diagnosis in case of myxoma suspicion at echocardiography. A confirmation is required before initiating an anticoagulation therapy, especially because there is no evidence that anticoagulant

therapy can prevent embolic events in myxomas [63]. Clinical context includes left or right atrial dilatation, heart failure with reduced ejection fraction, presence of central venous catheter or pacemaker (RA). Thrombi exceptionally have an IAS attachment [64]. If present on the posterior or lateral wall of the LA, it may cause difficulties in differentiating between a thrombus and a myxoma [11]. Thrombus has a low mobility and a sessile shape (Fig. 16). At CMR, T1w and T2w signal characteristics vary depending on the age of the thrombus. Thrombi are frequently isointense or hypointense at T1w, T2w and cine imaging, except in rare cases of acute thrombus or chronic organized thrombus. The Look Locker sequence to determine the optimal inversion time for LGE [65] may be helpful to differentiate between myxoma and thrombus [66–68]. Indeed, a thrombus has

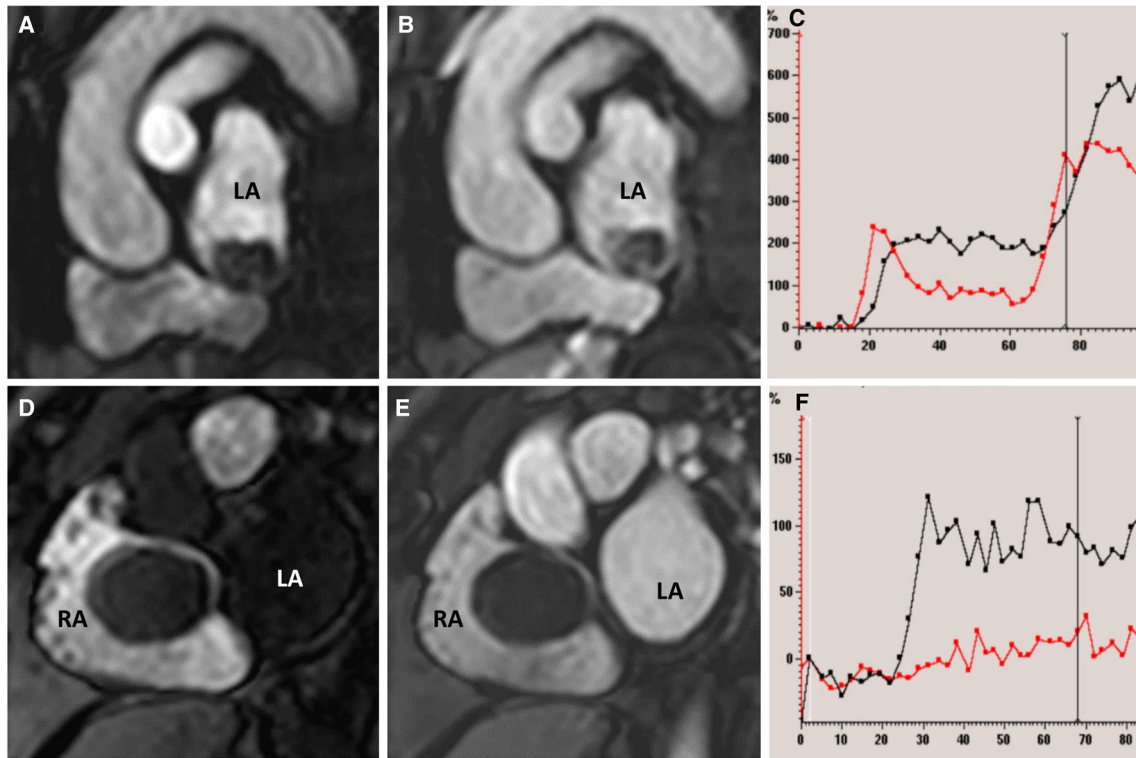


Fig. 11 First-pass perfusion differences between a highly (a–c) and a poorly (d–f) vascularized myxoma. A highly vascularized myxoma demonstrated higher signal at the myocardial phase images (b) compared to ventricular phase images (a) (LA=left atrium). The time-intensity curve (c) of myxoma (red curve) was quite similar

(although inferior) to adjacent normal myocardium (black curve). On the opposite, about one-half of myxoma are poorly vascularized with no enhancement between ventricular (d) and myocardial phases (e) (RA=right atrium). On the time-intensity curve, the perfusion of myxoma (red curve) remained very weak (f)

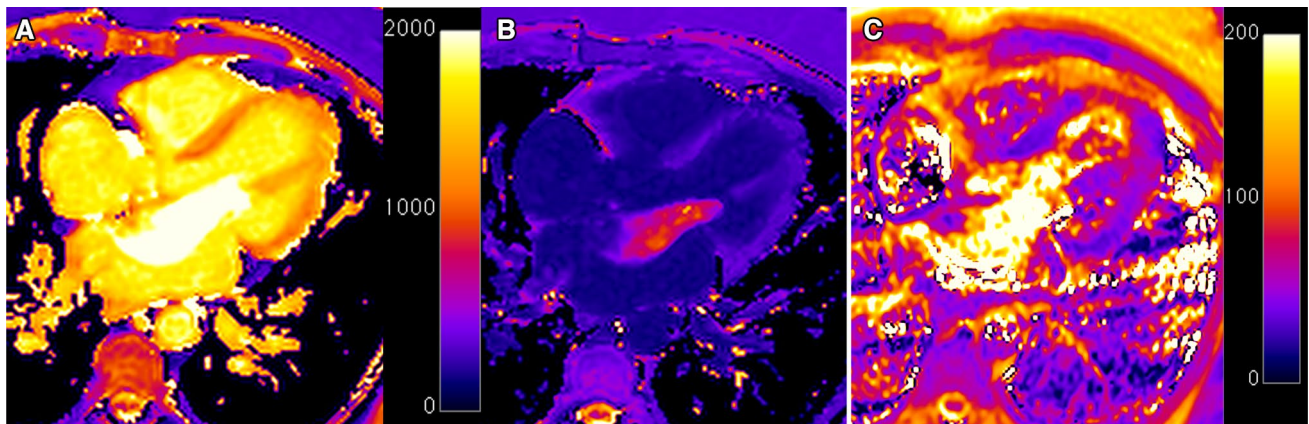


Fig. 12 The use of parametric sequence in myxoma represented in Fig. 3 revealed a native T1 time of 2185 ms (T1 mapping, a) in the most representative part of the tumor (3T system). Despite no obvious contrast enhancement was seen on LGE images, there was a 60%

drop in T1 time post gadolinium injection (840 ms, b). The extracellular volume of cardiac myxoma was 11%. Also, the tumor had a T2 time of 240 ms (T2 mapping, c), in accordance in high water content (myxoid matrix)

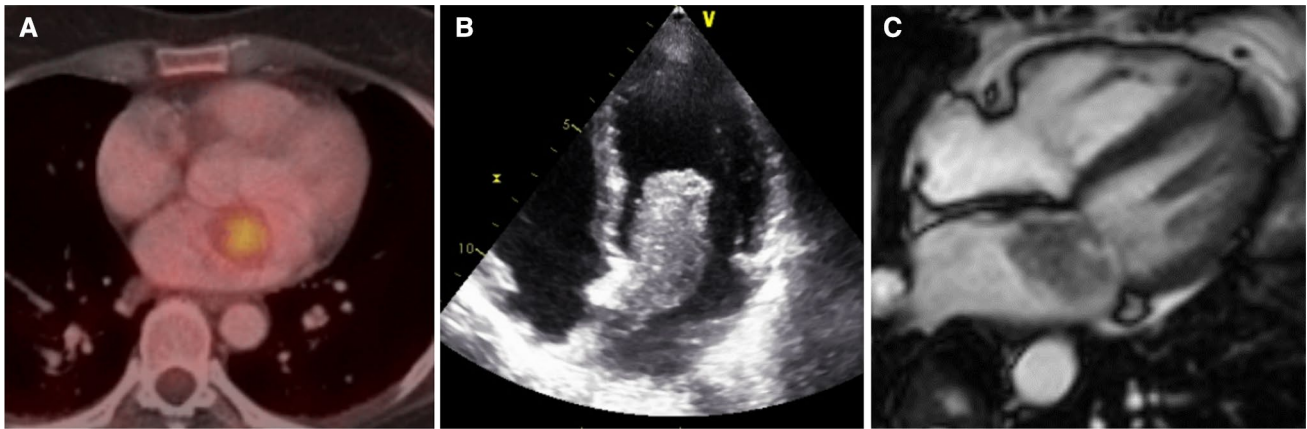


Fig. 13 A 56-year-old woman with fever and weight loss for several months. ^{18}F -FDG PET/CT solely revealed a mildly ^{18}F -FDG uptake area in the left atrium (a). TTE (b) and CMR (c) showed a left atrial pedunculated mass suggestive for myxoma

Table 2 Differential diagnosis of cardiac myxoma with interatrial septum attachment

Lipomatous hyperplasia of the interatrial septum

Typically elderly population
Dumbbell shaped appearance
Signal characteristics at CMR, attenuation characteristic at CT

Thrombi

Context: atrial (severe) dilatation, atrial fibrillation, deep venous line or pacemaker
Very rarely attached to the IAS
CMR: low signal at T2-weighted imaging; signal characteristics at LGE imaging

Metastasis

Context of known malignancy often present
Very rarely attached to the IAS
CMR presentation depends on malignancy etiology

Lymphoma/choroma

Location often not limited to the IAS with extending to the atrioventricular grooves; sometimes extending through more diffusely in the LA wall
Infiltrative > nodular, not mobile
CMR: homogenous > heterogeneous; isointense at T2-weighted imaging
PET: often high ^{18}F -FDG uptake (lymphoma)

Infectious/inflammatory disease (tuberculosis, granulomatosis with polyangiitis)

Infiltrative > nodular, not mobile
Pericardial enhancement / involvement
CMR: high enhancement at perfusion imaging
PET: often high ^{18}F -FDG uptake

Pheochromocytoma-paraganglioma

No intracavitary but extracardiac mass often located at the roof of IAS/LA
 ^{123}I -MIBG uptake

Lipoma

Rounded appearance
Typical signal characteristics at CMR

MIBG meta-iodobenzylguanidine

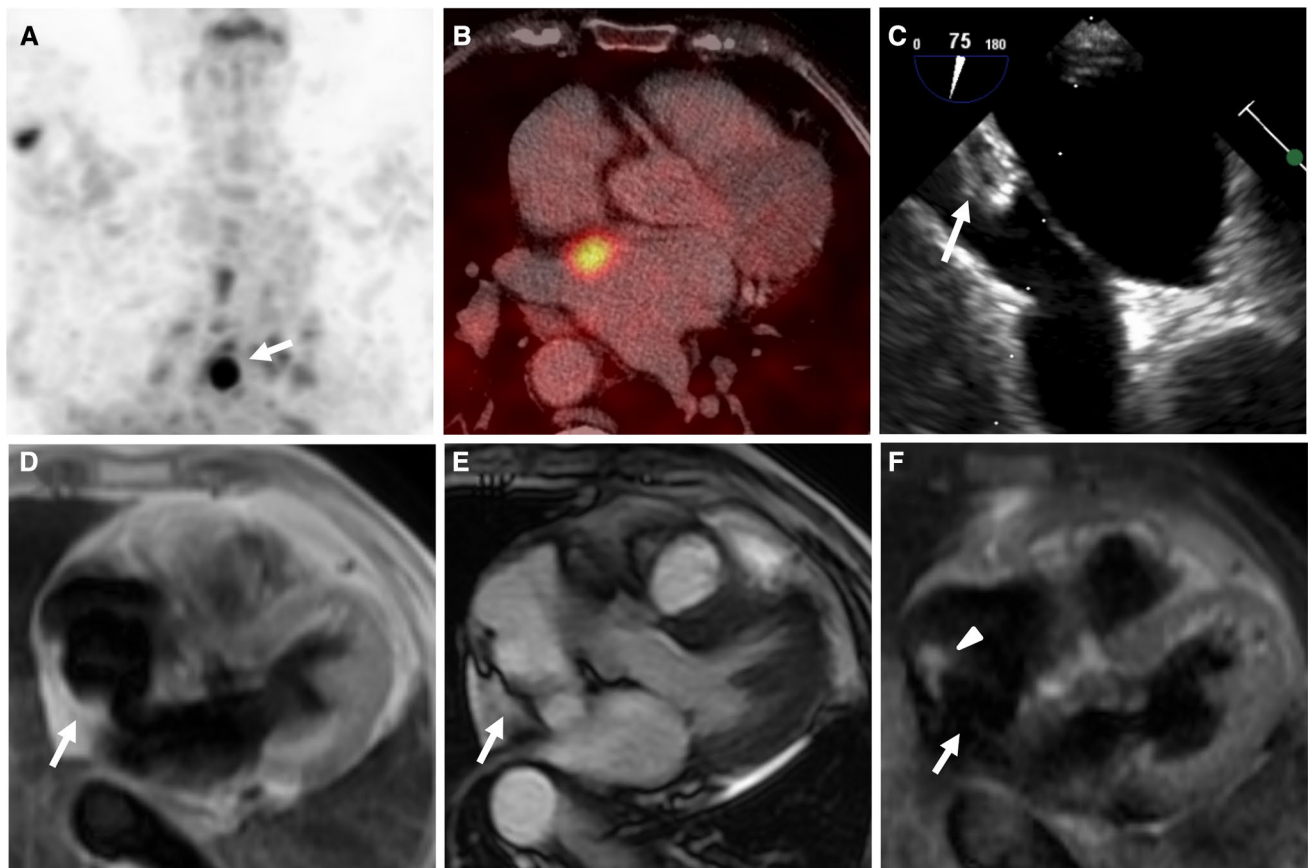


Fig. 14 Lipomatous hypertrophy of the interatrial septum. 77-year-old woman with history of breast cancer. ^{18}F -FDG PET/CT showed intense uptake in the interatrial septum (IAS) with a SUV at 10.7 (**a, b**). TEE showed heterogenous hyperechoic mass on the posterior part of the IAS (**c**, arrows) with suspected cardiac metastasis. CMR showed thickened IAS but no cardiac mass. The presence of fat was

well demonstrated with a high signal intensity at T1w (**d**) and cine (**e**) imaging and low signal intensity after fat signal suppression at T2w STIR imaging (**f**). Also note the prominent crista terminalis (**f**, arrowhead). Final cancer staging was no distant metastasis and was confirmed during the follow-up

an “edge” appearance at inversion times between 240 and 330 ms but becomes hypointense at longer inversion time (550–600 ms). In case of remaining doubt, cardiac thrombi show no ^{18}F -FDG uptake at PET/CT imaging [69].

Cardiac tumors Cardiac metastasis are more frequent than primary cardiac tumors [70] and a history of cancer is not always present (Fig. 17). Presentation depends on the type of spread and the histology. At CMR, metastasis features include frequent necrosis, pericardial enhancement or presence of lung metastasis. Fortunately cardiac metastasis with an IAS attachment is extremely rare, facilitating differential diagnosis [71]. Differentiation with the two most common primary malignant tumors, i.e. cardiac

angiosarcoma and primary cardiac lymphoma, is usually straightforward as their presentation is different. As CMR is superior to evaluate tumor location, and extent as well as tissue characterization, this technique is highly valuable [72]. Other histological types of primary cardiac sarcomas are not infrequently located in the LA and thus more likely to be confused with CM [73, 74]. Luckily there rarely have an IAS origin [75–77]. However, as these tumors are very rare, the value with regard to the role of CMR is limited [78]. Other masses, that may be located in the vicinity of IAS include benign cardiac tumor such as hemangioma or paraganglioma, and cystic structures such as bronchogenic cyst. These tumors may have an IAS origin [79–81] and

Fig. 15 Mitral valve annulus caseous calcification/necrosis. A 70-year-old patient was referred to our hospital for suspicion of left atrial sarcoma. TTE showed a highly echogenic mass attached to the mitral valve (a). CMR showed a homogenous mass hypointense at T1w (b) and T2w (c) imaging (arrowheads). A calcified mass was suspected and confirmed by CT (d)



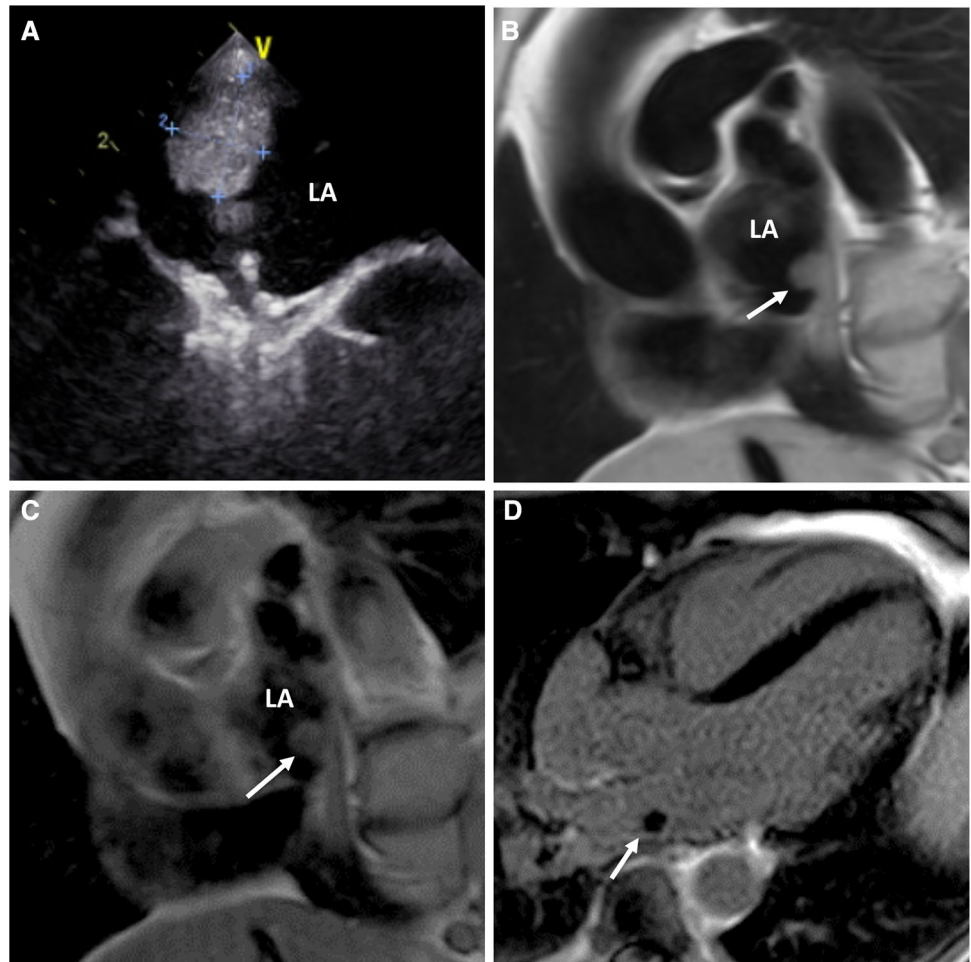
may become symptomatic, especially with arrhythmias or conduction disturbances (AV block) [82] necessitating surgical resection.

Inflammatory and infectious processes Inflammatory tumors as granulomatosis (with polyangiitis) or infectious processes as tuberculosis may involve the IAS [14, 83]. Histiocytic diseases as Erdheim-Chester disease may have a RA mass presentation [84]. These pseudotumors may have a malignant appearance because they are frequently infiltrative (wall thickening at echocardiography) with pericardial enhancement at CMR and high ^{18}F -FDG uptake at PET.

Rationalization in the multimodality imaging world: do we need anything more than echocardiography?

Echocardiography remains the imaging technique with the best spatial and temporal resolution. Its performance is excellent for myxoma detection and precision of its attachment point, particularly with TEE. Diagnosis of myxoma is based on a likelihood knowledge considering the prevalence and localization of myxoma. Therefore, one could wonder if another imaging modality is really needed. In clinical practice, echocardiography restrictions are related to its limited tissue characterization [85] and to the lack of paracardial environment information (Table 3; Fig. 17).

Fig. 16 Left atrial thrombus in a 55-year-old man with history of atrial septal defect closure device. TEE showed a small sessile mass attached to posterior left atrial wall (a). Cardiac MRI showed a small homogeneous mass isointense at T1w (b) and T2w (c) imaging. LGE imaging showed no enhancement (d). Because myxoma was not definitely excluded, surgical resection of the mass was performed and revealed a chronic, organized thrombus



Diagnostic uncertainty with regard to the diagnosis of CM at echocardiography happens in up 30% of cases [14] and are associated with absence of IAS attachment, absence of narrow stalk (sessile tumors) [34, 42, 86], history of cancer (doubt with metastasis), atypical echocardiographic presentation, i.e. cystic appearance, circumstances in which a thrombus may be suspected and more rarely poor acoustic windows. In these atypical presentations, further investigations are needed with additional imaging techniques. CMR shows several characteristics that are helpful to confidently characterize myxomas. CMR has proven its added value in the management of cardiac masses [47, 87–90], providing more correct histopathologic diagnoses compared to echocardiography [91]. However, some CMR limitations must be known. Because imaging is performed

during several heart beats, artefacts can occur when tumor motion is not reproducible between heartbeats. Limitations of CMR include tissue characterization (and even detection) of small masses (below 15 mm), especially when mobile, image quality in poorly collaborative patients or arrhythmia and some overlap in CM and thrombus presentation [61]. Even if experience is limited and overlap may occur between benign and malignant cardiac masses, ^{18}F -FDG PET/CT might have its interest in selected cases especially when a history of cancer is present or in when CMR is contraindicated or non-conclusive. CT also offers an alternative second-line imaging strategy useful (and also often easily available) to (1) exclude a cancer or (2) to demonstrate the presence of fat or calcifications. An

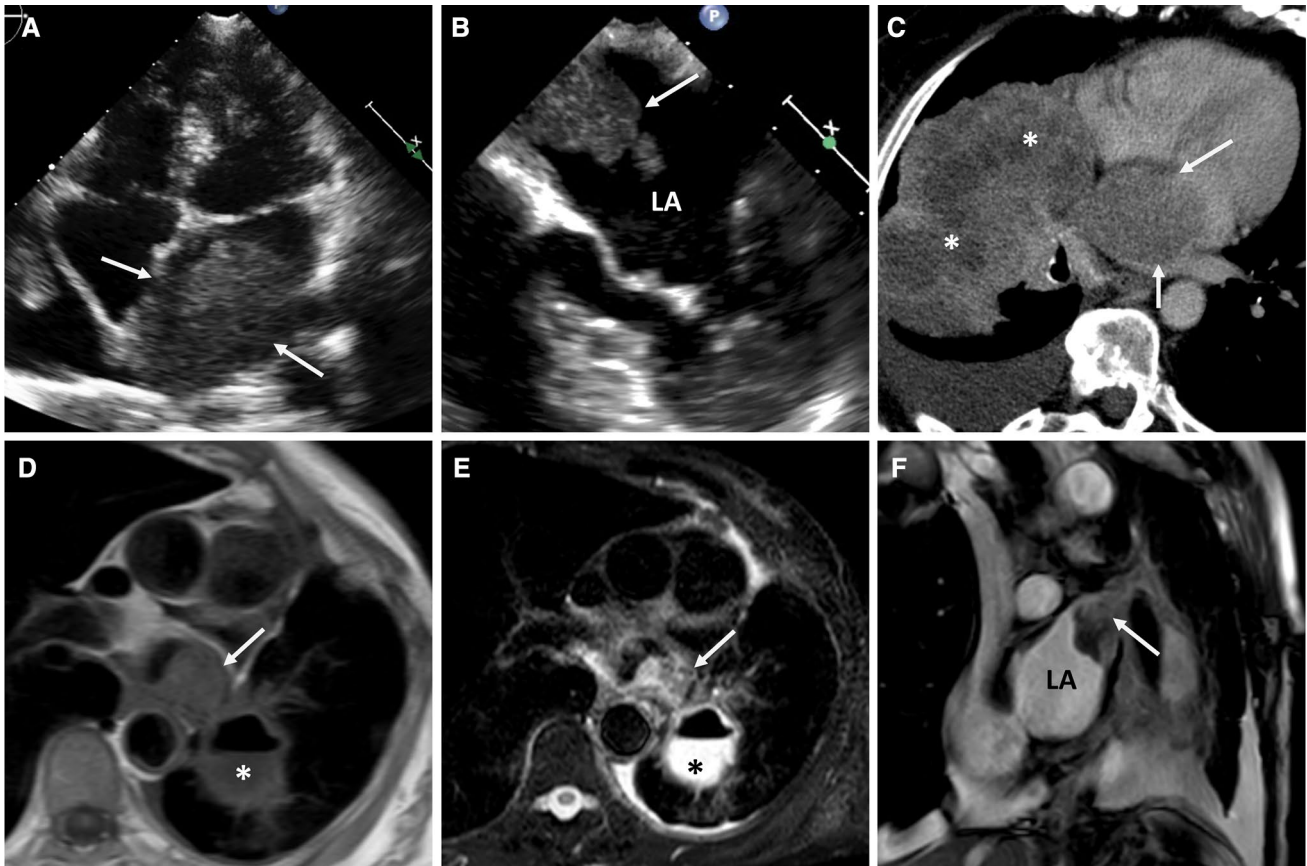


Fig. 17 Cardiac metastasis by direct invasion by lung carcinoma. (a–c) 73-year-old woman with dyspnea and no cancer history. TTE (a) revealed a mobile mass in the left atrium (LA). No interatrial septum attachment could be demonstrated, also at TEE (b). Diagnosis of myxoma was suspected and a surgical resection was initially scheduled. Because of chest X-ray abnormalities, a contrast-enhanced CT

was performed, revealing a lung cancer (*) with metastasis in the LA (arrows) by direct invasion of the right inferior pulmonary vein (c). (d–f) 63-year-old woman with necrotized lung carcinoma (*) invading the LA (arrows) via the pulmonary vein at T1w (d), T2w (e) and cine imaging (f, oblique sagittal view)

algorithm for how to choose which imaging modality is proposed in Fig. 18.

Conclusion

Due to the variability in location, shape, composition and vascularization, a confident diagnosis of CM is not always simple in daily practice. When the diagnostic likelihood is high based on echocardiography only (LA localization, IAS

attachment and mobility), additional imaging is optional. But, if the diagnosis is not clear/definite, further characterization of the cardiac mass is needed. With its good tissue characterization, CMR provides substantial information on the mass and helps the cardiologist in the management of cardiac masses. With the development of parametric sequences, CMR has a bright future by moving ever closer to histology.

Table 3 Advantages and limitation of cardiac imaging modality for cardiac myxoma diagnosis

	Advantages	Limitation
Echocardiography	Easily available High spatial resolution (TEE > TTE), detection of small mass High temporal resolution Functional and hemodynamic repercussions, underlying heart disease	Patient-dependent (echogenicity) Restricted field of view Poor tissue characterization
CMR	3D visualization Tissue characterization (differential diagnosis) Large field of view Moderate temporal resolution	Limited availability Average spatial resolution Reduced ability to characterize small and highly mobile masses Long examination time Patient-dependent (rhythm and collaboration) Contraindications (metal implants, renal failure)
CT	3D visualization Fast acquisition Easy available Spatial resolution Chest wall (robotic surgery)	Radiation exposure, even more when ECG-gated Low temporal resolution Average tissue characterization, except for fat and calcification Contraindications (renal failure)
¹⁸ F-FDG PET/CT	Large field of view Exclusion of secondary malignant tumors	Limited availability Poor spatial and temporal resolution Limited ability to differentiate other diseases (pseudotumors, benign tumors or infectious/inflammatory tumors)

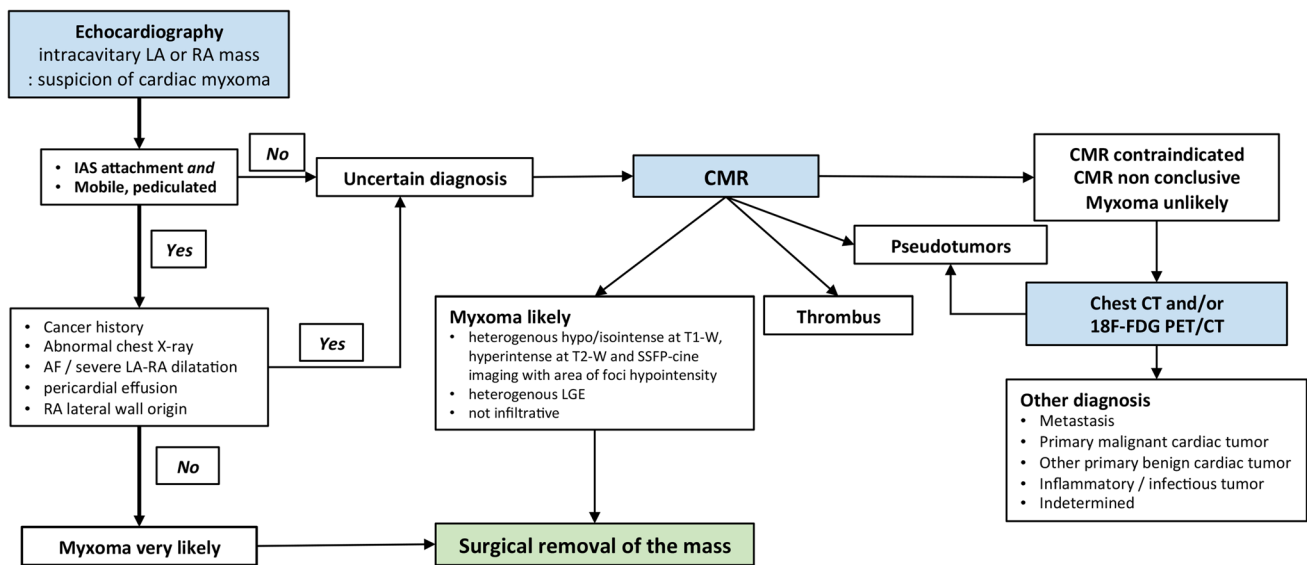


Fig. 18 Proposed Diagnostic Imaging Algorithm for suspicion of cardiac myxoma

Acknowledgements We thank Delphine Hoton (MD) for providing histological analysis and pictures of resected myxomas.

Compliance with ethical standards

Conflict of interest The authors declared that they have no conflict of interest.

References

1. Prichard RW (1951) Tumors of the heart; review of the subject and report of 150 cases. *AMA Arch Pathol* 51(1):98–128
2. Burke AP, Virmani R (1993) Cardiac myxoma. A clinicopathologic study. *Am J Clin Pathol* 100(6):671–680
3. Basso C, Valente M, Poletti A, Casarotto D, Thiene G (1997) Surgical pathology of primary cardiac and pericardial tumors. *Eur J Cardiothorac Surg* 12(5):730–737 discussion 7–8.

4. Reynen K (1995) Cardiac myxomas. *N Engl J Med* 333(24):1610–1617
5. Cina SJ, Smialek JE, Burke AP, Virmani R, Hutchins GM (1996) Primary cardiac tumors causing sudden death: a review of the literature. *Am J Forensic Med Pathol* 17(4):271–281
6. Goldberg HP, Glenn F, Dotter CT, Steinberg I (1952) Myxoma of the left atrium; diagnosis made during life with operative and post-mortem findings. *Circulation* 6(5):762–767
7. St John Sutton MG, Mercier LA, Giuliani ER, Lie JT. Atrial myxomas: a review of clinical experience in 40 patients. *Mayo Clin Proc.* 1980;55(6):371–6
8. Elbardissi AW, Dearani JA, Daly RC, Mullany CJ, Orszulak TA, Puga FJ et al (2008) Survival after resection of primary cardiac tumors: a 48-year experience. *Circulation* 118(14 Suppl):S7–15
9. Baris VO, Uslu A, Gerede DM, Kilickap M (2016) Rare cause of dyspnoea: pulmonary artery myxoma. *Eur Heart J Cardiovasc Imaging* 17(8):946
10. Pinede L, Duhaut P, Loire R (2001) Clinical presentation of left atrial cardiac myxoma. A series of 112 consecutive cases. *Medicine (Baltimore)* 80(3):159–172
11. Scheffel H, Baum Mueller S, Stolzmann P, Leschka S, Plass A, Alkadhhi H et al (2009) Atrial myxomas and thrombi: comparison of imaging features on CT. *AJR Am J Roentgenol* 192(3):639–645
12. Hong YJ, Hur J, Kim YJ, Lee HJ, Hong SR, Suh YJ et al (2014) Dual-energy cardiac computed tomography for differentiating cardiac myxoma from thrombus. *Int J Cardiovasc Imaging* 30(Suppl 2):121–128
13. Ha JW, Kang WC, Chung N, Chang BC, Rim SJ, Kwon JW et al (1999) Echocardiographic and morphologic characteristics of left atrial myxoma and their relation to systemic embolism. *Am J Cardiol* 83(11):1579–1582 A8.
14. Colin GC, Dymarkowski S, Gerber B, Michoux N, Bogaert J (2016) Cardiac myxoma imaging features and tissue characteristics at cardiovascular magnetic resonance. *Int J Cardiol* 202:950–951
15. Zheng Z, Guo G, Xu L, Lei L, Wei X, Pan Y (2014) Left atrial myxoma with versus without cerebral embolism: length of symptoms, morphologic characteristics, and outcomes. *Tex Heart Inst J* 41(6):592–595
16. Oliveira R, Branco L, Galrinho A, Abreu A, Abreu J, Fiarresga A et al (2010) Cardiac myxoma: a 13-year experience in echocardiographic diagnosis. *Rev Port Cardiol* 29(7–8):1087–1100
17. Malekzadeh S, Roberts WC (1989) Growth rate of left atrial myxoma. *Am J Cardiol* 64(16):1075–1076
18. Lane GE, Kapples EJ, Thompson RC, Grinton SF, Finck SJ (1994) Quiescent left atrial myxoma. *Am Heart J* 127(6):1629–1631
19. Ullah W, McGovern R (2005) Natural history of an atrial myxoma. *Age Ageing* 34(2):186–188
20. Karlof E, Salzberg SP, Anyanwu AC, Steinbock B, Filsoufi F (2006) How fast does an atrial myxoma grow? *Ann Thorac Surg* 82(4):1510–1512
21. Burke A, Virmani R (1996) More on cardiac myxomas. *N Engl J Med* 335(19):1462–1463 author reply 3–4.
22. Effert S, Domanig E (1959) Diagnosis of intra-auricular tumors & large thrombi with the aid of ultrasonic echography. *Dtsch Med Wochenschr* 84(1):6–8
23. Lackner K, Heuser L, Friedmann G, Thurn P. Computer cardio-tomography for tumours of the left atrium *Rofo.* 1978;129(6):735–739
24. Amparo EG, Higgins CB, Farmer D, Gamsu G, McNamara M (1984) Gated MRI of cardiac and paracardiac masses: initial experience. *AJR Am J Roentgenol* 143(6):1151–1156
25. Agostini D, Babatasi G, Galateau F, Grollier G, Potier JC, Bouvard G (1999) Detection of cardiac myxoma by F-18 FDG PET. *Clin Nucl Med* 24(3):159–160
26. Engberding R, Daniel WG, Erbel R, Kasper W, Lestuzzi C, Curtius JM et al (1993) Diagnosis of heart tumours by transoesophageal echocardiography: a multicentre study in 154 patients. *European Cooperative Study Group. Eur Heart J* 14(9):1223–1228
27. Marshall WH Jr, Steiner RM, Wexler L (1969) “Tumor vascularity” in left atrial myxoma demonstrated by selective coronary arteriography. *Radiology* 93(4):815–816 passim
28. Rahmanian PB, Castillo JG, Sanz J, Adams DH, Filsoufi F (2007) Cardiac myxoma: preoperative diagnosis using a multimodal imaging approach and surgical outcome in a large contemporary series. *Interact Cardiovasc Thorac Surg* 6(4):479–483
29. Van Cleemput J, Daenen W, De Geest H (1993) Coronary angiography in cardiac myxomas: findings in 19 consecutive cases and review of the literature. *Cathet Cardiovasc Diagn* 29(3):217–220
30. Furedi GA, Knechtges TE, Czarnecki DJ (1989) Coronary angiography in atrial myxoma: findings in nine cases. *AJR Am J Roentgenol* 152(4):737–738
31. Hwang JJ, Lien WP, Kuan P, Hung CR, How SW (1991) Atypical myxoma. *Chest* 100(2):550–551
32. Park KJ, Woo JS, Park JY (2013) Left atrial myxoma presenting with unusual cystic form. *Korean J Thorac Cardiovasc Surg* 46(5):362–364
33. Handke M, Goepfrich M, Keller H (2008) Strongly neovascularized left atrial myxoma. *Eur J Echocardiogr* 9(1):99–100
34. Obeid AI, Marvasti M, Parker F, Rosenberg J (1989) Comparison of transthoracic and transesophageal echocardiography in diagnosis of left atrial myxoma. *Am J Cardiol* 63(13):1006–1008
35. Mugge A, Daniel WG, Haverich A, Lichtlen PR (1991) Diagnosis of noninfective cardiac mass lesions by two-dimensional echocardiography. Comparison of the transthoracic and transesophageal approaches. *Circulation* 83(1):70–78
36. Leibowitz G, Keller NM, Daniel WG, Freedberg RS, Tunick PA, Stottmeister C et al (1995) Transesophageal versus transthoracic echocardiography in the evaluation of right atrial tumors. *Am Heart J* 130(6):1224–1227
37. Kirkpatrick JN, Wong T, Bednarz JE, Spencer KT, Sugeng L, Ward RP et al (2004) Differential diagnosis of cardiac masses using contrast echocardiographic perfusion imaging. *J Am Coll Cardiol* 43(8):1412–1419
38. Mansencal N, Revault-d’Allonnes L, Pelage JP, Farcot JC, Lacombe P, Dubourg O (2009) Usefulness of contrast echocardiography for assessment of intracardiac masses. *Arch Cardiovasc Dis* 102(3):177–183
39. Strachinaru M, Damry N, Duttman R, Wauthy P, Catez E, Lutea M et al (2016) Ultrasound Contrast Quantification for the Diagnosis of Intracardiac Masses. *JACC Cardiovasc Imaging* 9(6):747–750
40. Muller S, Feuchtner G, Bonatti J, Muller L, Laufer G, Hiemetzberger R et al (2008) Value of transesophageal 3D echocardiography as an adjunct to conventional 2D imaging in preoperative evaluation of cardiac masses. *Echocardiography* 25(6):624–631
41. Semelka RC, Shoenut JP, Wilson ME, Pellech AE, Patton JN (1992) Cardiac masses: signal intensity features on spin-echo, gradient-echo, gadolinium-enhanced spin-echo, and TurboFLASH images. *J Magn Reson Imaging* 2(4):415–420
42. Araoz PA, Mulvagh SL, Tazelaar HD, Julsrud PR, Breen JF (2000) CT and MR imaging of benign primary cardiac neoplasms with echocardiographic correlation. *Radiographics* 20(5):1303–1319
43. Grebenc ML, Rosado-de-Christenson ML, Green CE, Burke AP, Galvin JR (2002) Cardiac myxoma: imaging features in 83 patients. *Radiographics* 22(3):673–689
44. Sparrow PJ, Kurian JB, Jones TR, Sivananthan MU (2005) MR imaging of cardiac tumors. *Radiographics* 25(5):1255–1276

45. Motwani M, Kidambi A, Herzog BA, Uddin A, Greenwood JP, Plein S (2013) MR imaging of cardiac tumors and masses: a review of methods and clinical applications. *Radiology* 268(1):26–43
46. Masui T, Takahashi M, Miura K, Naito M, Tawarahara K (1995) Cardiac myxoma: identification of intratumoral hemorrhage and calcification on MR images. *AJR Am J Roentgenol* 164(4):850–852
47. Fussen S, De Boeck BW, Zellweger MJ, Bremerich J, Goetschalckx K, Zuber M et al (2011) Cardiovascular magnetic resonance imaging for diagnosis and clinical management of suspected cardiac masses and tumours. *Eur Heart J* 32(12):1551–1560
48. Bauner KU, Sourbron S, Picciolo M, Schmitz C, Theisen D, Sandner TA et al (2012) MR first pass perfusion of benign and malignant cardiac tumours—significant differences and diagnostic accuracy. *Eur Radiol* 22(1):73–82
49. Mohrs OK, Voigtlaender T, Petersen SE, Zander M, Schulze T, Pottmeyer A et al (2008) First experiences with contrast-enhanced first-pass MR perfusion imaging in patients with primary, benign cardiac masses and tumour-like lesions. *Eur Radiol* 18(8):1617–1624
50. Caspar T, El Ghannudi S, Ohana M, Labani A, Lawson A, Ohlmann P et al (2017) Magnetic resonance evaluation of cardiac thrombi and masses by T1 and T2 mapping: an observational study. *Int J Cardiovasc Imaging* 33(4):551–559
51. Kubler D, Grafe M, Schnackenburg B, Knosalla C, Wassilew K, Hassel JH et al (2013) T1 and T2 mapping for tissue characterization of cardiac myxoma. *Int J Cardiol* 169(1):e17–e20
52. Shin W, Choe YH, Kim SM, Song IY, Kim SS (2014) Detection of cardiac myxomas with non-contrast chest CT. *Acta Radiol* 55(3):273–278
53. Gheysens O, Cornillie J, Voigt JU, Bogaert J, Westhovens R (2013) Left atrial myxoma on FDG-PET/CT. *Clin Nucl Med* 38(11):e421–e422
54. Okazaki Y, Yamada S, Kitada S, Matsunaga I, Nogami E, Watanabe T et al (2014) Significance of 18 F-FDG PET and immunohistochemical GLUT-1 expression for cardiac myxoma. *Diagnostic pathology* 9:117
55. Rahbar K, Seifarth H, Schafers M, Stegger L, Hoffmeier A, Spieker T et al (2012) Differentiation of malignant and benign cardiac tumors using 18F-FDG PET/CT. *J Nucl Med* 53(6):856–863
56. Nensa F, Tezgah E, Poeppel TD, Jensen CJ, Schelhorn J, Kohler J et al (2015) Integrated 18F-FDG PET/MR imaging in the assessment of cardiac masses: a pilot study. *J Nucl Med* 56(2):255–260
57. Kuester LB, Fischman AJ, Fan CM, Halpern EF, Aquino SL (2005) Lipomatous hypertrophy of the interatrial septum: prevalence and features on fusion 18F fluorodeoxyglucose positron emission tomography/CT. *Chest* 128(6):3888–3893
58. Manabe O, Oyama-Manabe N, Alisa K, Hirata K, Itoh K, Terae S et al (2012) Multimodality evaluation of cardiac paraganglioma. *Clin Nucl Med* 37(6):599–601
59. Colin GC, Vancraeynest D, Hoton D, Jonard P, Gerber B (2015) Complete heart block caused by diffuse pseudotumoral cardiac involvement in granulomatosis with polyangiitis. *Circulation* 132(17):e207–e210
60. Keeling IM, Oberwalder P, Anelli-Monti M, Schuchlenz H, Demel U, Tilz GP et al (2002) Cardiac myxomas: 24 years of experience in 49 patients. *Eur J Cardiothorac Surg* 22(6):971–977
61. Tamma R, Dong W, Wang J, Litt H, Han Y (2016) Evaluation of cardiac masses by CMR—strengths and pitfalls: a tertiary center experience. *Int J Cardiovasc Imaging* 32(6):913–920
62. Hoey ET, Mankad K, Puppala S, Gopalan D, Sivananthan MU (2009) MRI and CT appearances of cardiac tumours in adults. *Clin Radiol* 64(12):1214–1230
63. Knepper LE, Biller J, Adams HP Jr, Bruno A (1988) Neurologic manifestations of atrial myxoma. A 12-year experience and review. *Stroke* 19(11):1435–1440
64. Chen MA, Ahlgrim AA, Allen CT (2009) Location, location, location: a left atrial mass. *J Am Soc Echocardiogr* 22(5):541.e3–541.e4
65. Pazos-Lopez P, Pozo E, Siqueira ME, Garcia-Lunar I, Cham M, Jacobi A et al (2014) Value of CMR for the differential diagnosis of cardiac masses. *JACC Cardiovasc Imaging* 7(9):896–905
66. Heitner JF, Klem I, Alexander K, Thomson L, Meine TJ, Patel MR et al (2005) The case of the disappearing myxoma. *J Cardiovasc Magn Reson* 7(5):841–843
67. Mollet NR, Dymarkowski S, Volders W, Wathiong J, Herbots L, Rademakers FE et al (2002) Visualization of ventricular thrombi with contrast-enhanced magnetic resonance imaging in patients with ischemic heart disease. *Circulation* 106(23):2873–2876
68. Abbas A, Garfath-Cox KA, Brown IW, Shambrook JS, Peebles CR, Harden SP (2015) Cardiac MR assessment of cardiac myxomas. *Br J Radiol* 88(1045):20140599
69. Rinuncini M, Zuin M, Scaranello F, Fejzo M, Rampin L, Rubello D et al (2016) Differentiation of cardiac thrombus from cardiac tumor combining cardiac MRI and 18F-FDG-PET/CT Imaging. *Int J Cardiol* 212:94–96
70. Butany J, Nair V, Naseemuddin A, Nair GM, Catton C, Yau T (2005) Cardiac tumours: diagnosis and management. *Lancet Oncol* 6(4):219–228
71. Kontozis L, Soteriou M, Papamichael D, Economides C, Bagdades E, Christou C et al (2011) Isolated right atrial metastasis of malignant melanoma mimicking a myxoma. *Hellenic J Cardiol* 52(3):281–284
72. Colin GC, Symons R, Dymarkowski S, Gerber B, Bogaert J. Value of CMR to Differentiate Cardiac Angiosarcoma From Cardiac Lymphoma. *JACC Cardiovasc Imaging*. 2014
73. Kilic ID, Alihanoglu YI, Ozcan AV, Taskoylu O, Bir F, Evrenkul H (2014) Huge leiomyosarcoma in the left atrium. *Herz* 39(4):538–539
74. Kuurstra EJ, Mullen JC, MacArthur RG (2014) Massive left atrial sarcoma presenting with severe congestive heart failure. *Can J Cardiol* 30(10):1250.e13–e5
75. Legault S, Couture C, Bourgault C, Bergeron S, Poirier P, Senéchal M (2009) Primary cardiac Burkitt-like lymphoma of the right atrium. *Can J Cardiol* 25(3):163–165
76. Peyrou J, Park CI, Cikirikcioglu M, Shah D, Muller H (2013) A rare cause of Bachmann interatrial block. *Eur Heart J Cardiovasc Imaging* 14(12):1131
77. Puppala S, Hoey ET, Mankad K, Wood AM (2010) Primary cardiac angiosarcoma arising from the interatrial septum: magnetic resonance imaging appearances. *Br J Radiol* 83(995):e230–e234
78. O'Donnell DH, Abbara S, Chaithiraphan V, Yared K, Killeen RP, Cury RC et al (2009) Cardiac tumors: optimal cardiac MR sequences and spectrum of imaging appearances. *AJR Am J Roentgenol* 193(2):377–387
79. Seo N, Kang JW, Lim CH, Kim B, Lee HJ, Lim TH (2011) CT findings of an intracardiac bronchogenic cyst. *Int J Cardiovasc Imaging* 27(5):701–704
80. Hrabak-Paar M, Hubner M, Stern-Padovan R, Lusic M (2011) Hemangioma of the interatrial septum: CT and MRI features. *Cardiovasc Intervent Radiol* 34(Suppl 2):S90-3
81. Butany J, Nair V, Ahluwalia MS, El Demellwy D, Siu S, Fiendel C (2004) Papillary fibroelastoma of the interatrial septum: a case report. *J Card Surg* 19(4):349–353
82. Borges AC, Knebel F, Lembcke A, Panda A, Komoda T, Hieemann NE et al (2009) Bronchogenic cyst of the interatrial septum presenting as atrioventricular block. *Ann Thorac Surg* 87(6):1920–1923

83. Taskesen T, Goldberg SL, Mannelli L, Rabkin D, Hawn TR, Fligner CL et al (2015) Granulomatosis with polyangiitis presenting with an intracardiac mass and complete heart block: enhanced images by 3-dimensional echocardiography. *Circulation* 132(10):961–964
84. Haroche J, Cluzel P, Toledano D, Montalescot G, Touitou D, Grenier PA et al (2009) Images in cardiovascular medicine. Cardiac involvement in Erdheim-Chester disease: magnetic resonance and computed tomographic scan imaging in a monocentric series of 37 patients. *Circulation* 119(25):e597–e598
85. Sugeng L, Lang RM (2004) Atypical cardiac myxomas. *Echocardiography* 21(1):43–47
86. Bruce CJ (2011) Cardiac tumours: diagnosis and management. *Heart* 97(2):151–160
87. Freedberg RS, Kronzon I, Rumancik WM, Liebeskind D (1988) The contribution of magnetic resonance imaging to the evaluation of intracardiac tumors diagnosed by echocardiography. *Circulation* 77(1):96–103
88. Gulati G, Sharma S, Kothari SS, Juneja R, Saxena A, Talwar KK (2004) Comparison of echo and MRI in the imaging evaluation of intracardiac masses. *Cardiovasc Intervent Radiol* 27(5):459–469
89. Winkler M, Higgins CB (1987) Suspected intracardiac masses: evaluation with MR imaging. *Radiology* 165(1):117–122
90. Patel R, Lim RP, Saric M, Nayar A, Babb J, Ettl M et al (2016) Diagnostic performance of cardiac magnetic resonance imaging and echocardiography in evaluation of cardiac and paracardiac masses. *Am J Cardiol* 117(1):135–140
91. Giusca S, Mereles D, Ochs A, Buss S, Andre F, Seitz S et al (2017) Incremental value of cardiac magnetic resonance for the evaluation of cardiac tumors in adults: experience of a high volume tertiary cardiology centre. *Int J Cardiovasc Imaging* 33(6):879–888